Compound diffractive telescope system: design, stray light analysis, and optical test*

Yue Jin-Ying(岳巾英)[a)b)], Liu Hua(刘 华)[a)], Lu Zhen-Wu(卢振武)[a)†], Xu Wen-Bin(许文斌)[a)b)], Zhang Hu(张 虎)[a)b)], Zhang Hong-Xin(张红鑫)[a)], and Liu Ying(刘 英)[a)b)]

[a)] *Opto-electonics Technology Center, Changchun Institute of Optics, Fine Mechanics and Physics, Changchun* 130033, *China*

[b)] *Graduate School of the Chinese Academy of Sciences, Beijing* 100039, *China*

(Received 27 February 2009; revised manuscript received 8 July 2009)

The compound diffractive telescope is a novel space optical system which combines the structure of compound eyes with diffractive optics and so it has a lighter weight, a wider field of view (FOV), a lower cost as well as looser fabrication tolerance. In this paper, the design of a compound diffractive telescope composed of one primary lens and twenty-one eyepieces is introduced. Then the influence of diffraction orders on the performance of the system is analysed. A modified phase function model of diffractive optics is proposed to analyse the modulation transfer function (MTF) curves for 0° FOV, which provides a more accurate prediction of the performance of the system. In addition, an optimized mechanism is also proposed to suppress stray light. The star image and resolution tests show that the system can achieve diffraction limit imaging within ±2° of FOV and ±4 mm of eccentricity. Finally, a series of pictures of an object are taken from different channels, and the splicing of pictures from adjacent FOVs is demonstrated. In summary, the designed system has been proved to have great potential applications.

Keywords: lens system design, compound eyes structure, diffractive lens, stray light

PACC: 0760, 4278F, 4215E, 4285F

1. Introduction

To solve the mass-and-launch ability problems, a membrane mirror[1,2] or a diffractive optical element[3,4] has been used to form an ultra-light weight telescope. However, both of these have disadvantages. For the system with the membrane mirror, the required surface precision is too high to be fabricated, while for the system with diffractive optics, the field of view (FOV) is normally restricted by the eyepiece. The compound diffractive telescope which combines the structure of compound eyes[5−8] with diffractive optics can cope well with these problems as this kind of telescope is lighter in weight, wider in FOV, lower in cost and looser in sensitivity to manufacturing tolerance.

In the present paper, the design of a compound diffractive telescope is introduced, which is composed of one primary lens and twenty-one eyepieces. The influence of diffraction orders of the primary lens on the system is analysed. The modulation transfer function (MTF) curve corresponding to 0° FOV is revised within the design spectrum range so that it can provide a more accurate prediction of the performance of the system. In addition, an optimized mechanical structure is proposed to suppress stray light. The performance of the system is tested by star image and resolution tests, and diffraction limit images are obtained within ±2° of FOV and ±4 mm of eccentricity. Finally, a series of target pictures are taken from different eyepieces, and the pictures taken from adjacent channels are spliced together. All of the results indicate that this novel telescope has a good performance.

2. General description of compound diffractive telescope

The compound diffractive telescope is composed of one hybrid refractive-diffractive lens, 21 eyepieces and CCDs. It works in a spectrum range from 0.4 μm to 0.7 μm. The structure of the system is shown in Fig. 1.

*Project supported by the National High Technology Research and Development Program of China (Grant No. 2006AA12Z127), the National Natural Science Foundation of China (Grant No. 10704072) and the Innovation Program of Chinese Academy of Sciences.

†Corresponding author. E-mail: luzhenwu55@yahoo.com.cn

© 2010 Chinese Physical Society and IOP Publishing Ltd

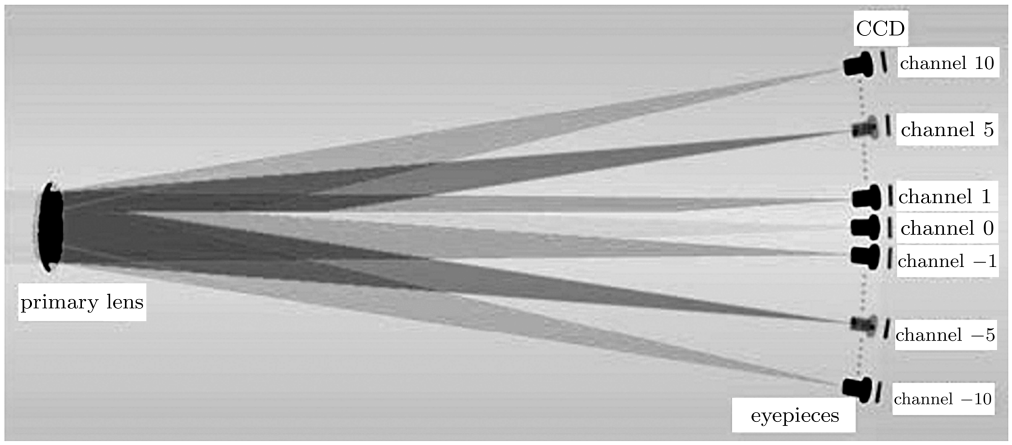


Fig. 1. Structure of the compound diffractive telescope.

The focal length $f(\lambda_i)$ for the diffractive element is dependent on design wavelength λ_0, design focal length f_0 and incident wavelength λ_i governed by the following formula:

$$f(\lambda_i) = f_0 \times \frac{\lambda_0}{\lambda_i}. \tag{1}$$

As the colour dispersion of a refractor is opposite in sign to that of a diffractor, a hybrid refractive-diffractive lens is used as a primary lens to correct chromatic aberration of the system. The aperture of the primary lens is 50 mm, with an F number of 49. The first surface of the primary lens is a planar surface in which a diffractive surface relief is etched, while the second surface is a spherical surface with a curvature radius of 1336.9 mm. Each eyepiece is composed of one doublet lens and two small single lenses, with a total length of 43 mm and an aperture of 8 mm. The 21 eyepieces are deployed by referring to the structure of the superposition compound eye of insects. If the eyepiece is located on the focus of the central working wavelength of the primary lens, it is defined as channel 0. Accordingly, the channel (+/−) n is defined by rotating channel 0 through an angle of (+/−) $n \times 0.2°$ around the principal optic axis of the primary lens. Since the FOV of the system is related to the number of channels, an extended FOV of 4.2° can be obtained with 21 eyepieces in design. The MTF curves for channel 0 and channel 10 are shown in Fig. 2. As can be seen, the MTF value is higher than 0.75 at 50 lp/mm for channel 0 and the MTF value is about 0.68 at 50 lp/mm for channel 10. Here lp means the line-pair.

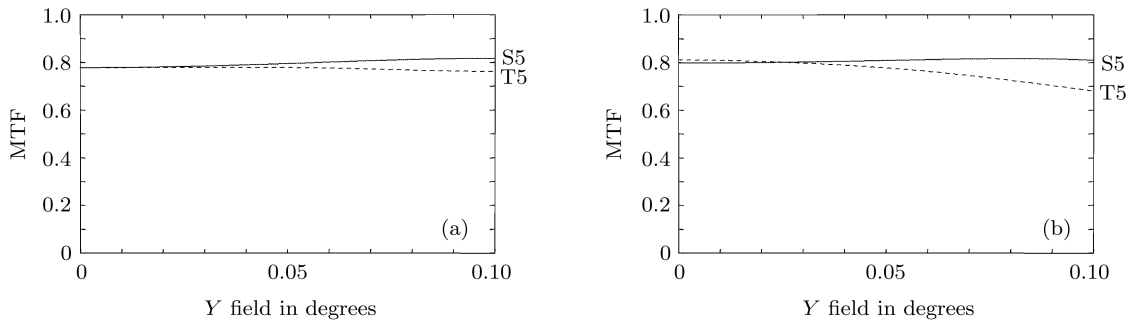


Fig. 2. (a) MTF plot of channel 0, (b) MTF plot of channel 10.

3. Simulation of system with advanced system analysis program (ASAP)

The diffraction efficiency[9] for a binary optical element depends on the diffraction order, incident angle of the light, wavelength and so on as shown by the following formulas:

$$\eta_m^N = \left\{ \frac{\sin[\pi(m-\phi)]}{\sin[\pi(m-\phi)/N]} \times \frac{\sin(\pi m/N)}{\pi m} \right\}^2, \quad (2)$$

$$\phi = \frac{\lambda_0}{\lambda_i} \times \frac{\sqrt{n_i^2 - \sin^2\theta} - \cos\theta}{n_0 - 1}, \quad (3)$$

where m is the diffraction order, N is the number of levels, n_0 is the refractive index of the substrate for the design wavelength of λ_0, n_i is the refractive index for λ_i, and θ is the incident angle. In the present part, the performance of the optical system is first analysed with ASAP, and then an optimized mechanical structure is proposed for the eyepiece.

3.1. Influence of diffraction order

Stray light produced by unwanted diffraction order of the diffractive primary lens received by the detector is first analysed with ASAP. For simplicity, a coherent diffractive beam is used to analyse the influence of diffraction order on energy, the reflection effect of the optical component is ignored, and the test surface is set to be 4 times the Airy disc in size. Typically, only three diffraction orders of the primary lens are assumed to account for all the incident energies. Two examples of the energy distribution on the detector are shown in Fig. 3.

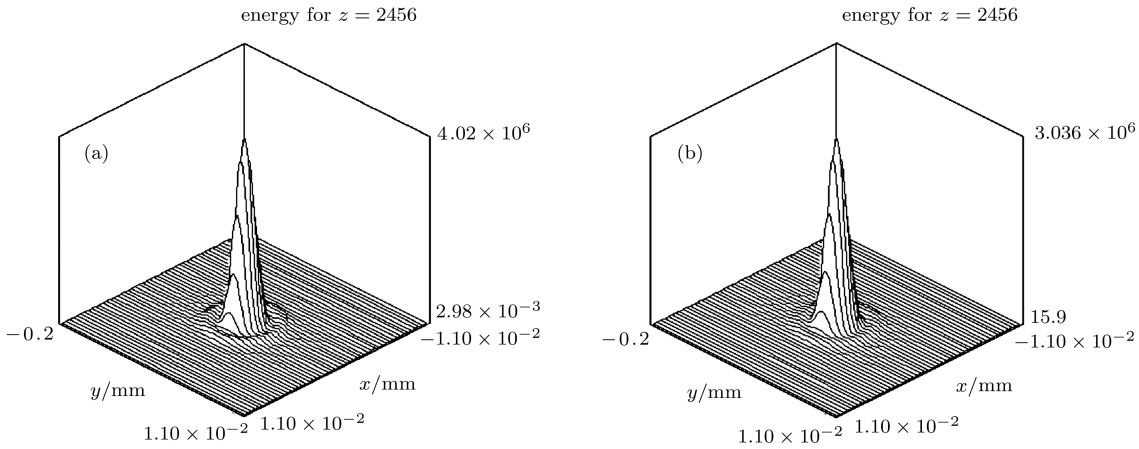


Fig. 3. (a) Airy disc with $\eta_{+1} = 100\%$, and (b) Airy disc with $\eta_{+1} = 95\%$, $\eta_0 = 2.5\%$ and $\eta_{+2} = 2.5\%$.

A traditional energy distribution of the Airy disc for the system is shown in Fig. 3(a), which does not consider the non-designed diffraction orders. As can be seen, the peak energy is 9 orders of magnitude higher than the valley energy. When the diffraction efficiency of the +1st diffraction order is set to be 95%, and both the 0th and +2nd diffracted efficiencies are set to be 2.5%, the modified energy distribution of the Airy disc will look like the one shown in Fig. 3(b). It can be seen clearly that the ratio of the P–V energy is reduced to 6 orders of magnitude by non-designed diffraction orders in this case. Therefore it can be concluded that the non-designed diffraction orders will affect the energy distribution of the Airy disc significantly.

Moreover, the influence of the diffraction orders[10,11] on the MTF of the system was also analysed. According to formula (2), the MTF curve corresponding to 0° FOV is revised within the design spectrum range, and the comparison result obtained with Zemax and Matlab under different conditions is shown in Fig. 4.

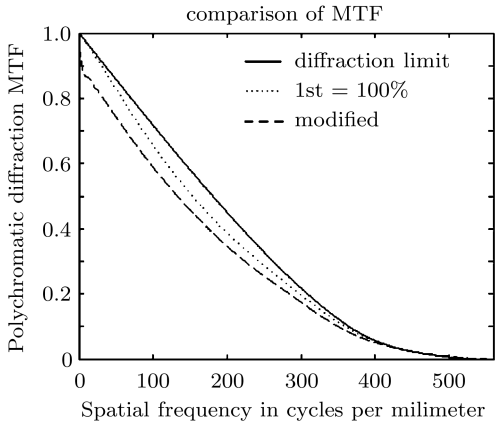


Fig. 4. Comparison between the MTF curves of the system under different conditions. The dot line is the traditional MTF curve with only the designed diffraction order of the +1st, while the dash line is the modified MTF curve considering the influence of the non-designed diffraction orders. The modified MTF value decreases obviously compared with the traditional MTF especially at low spatial frequency. We attribute the descent of the MTF value to the long distance (about 2416 mm) between the primary lens and the eyepiece.

3.2. Mechanism for eyepiece

Besides non-designed diffraction orders, the mechanical structure of the eyepiece is actually another important stray light source. The eyepiece initially consists of one external barrel, one inner barrel, one ordinary clamping ring, one gasket (for the last two small lenses) and a connecting shell for CCD. In the ASAP, the light is allowed to split twice according to Fresnel's law on an optical interface, and a reflective command is assigned to the mechanical components during an incoherent geometric ray-trace. For the convenience of comparison, the total energy of parent imaging rays and child stray rays finally arriving at the CCD is normalized to 1. As a result of the first ray-trace, it is found that the parent imaging rays occupy 98.47% of the energy, and the front surface of the doublet lens is the main reflection surface of the eyepiece. To reduce the stray light caused by the reflection, the mechanical structure of the eyepiece is optimized. Firstly, the aperture of the clamping ring is strictly shrunk to match the clear aperture of the doublet lens, which greatly reduces the entrance of the stray light into the detector. Secondly, a new filter with an aperture larger than the clear aperture of the singlet lens is added into the inner barrel appropriately. After the modification of the mechanical structure of the eyepiece, the second ray-trace is executed and the result shows that the energy of parent imaging rays is now increased to 98.89%. The first ray-trace of the system is shown in Fig. 5(a) and the magnified optical and mechanical structure of the eyepiece is shown in Fig. 5(b). For the second ray-trace, the optical paths are reduced significantly in the optimized eyepiece with the right clamping ring part A and the new filter part B shown in Fig. 5(c).

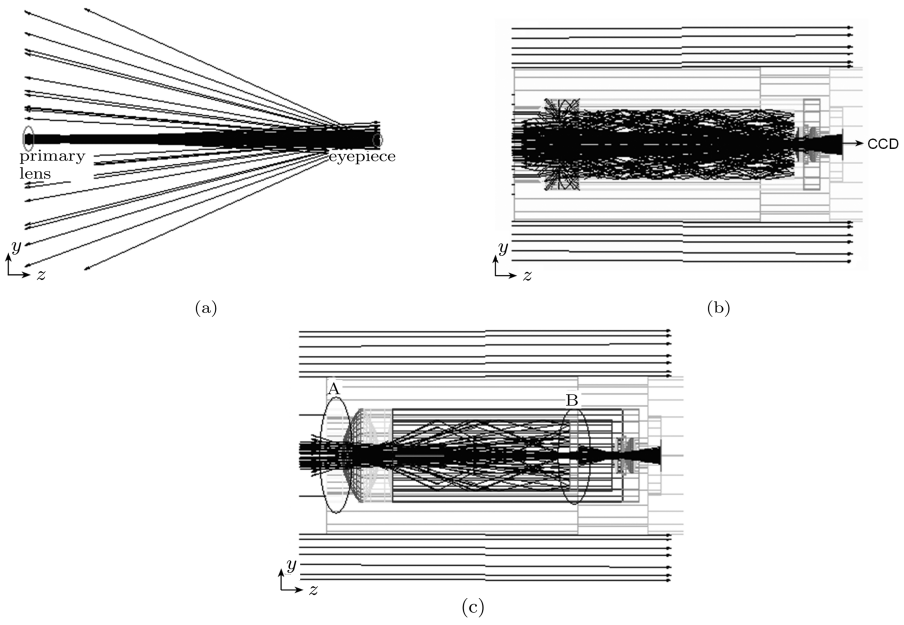


Fig. 5. (a) First incoherent geometric ray-trace of the system, (b) magnification of the eyepiece, and (c) second ray-trace for the optimized mechanism of the eyepiece.

4. Star image and resolution tests

The performance of the compound diffractive telescope is tested by star image and resolution tests. For the star image test[12,13] the optical setup is shown in Fig. 6, where a He–Ne laser with a 632.8 nm wavelength is located in front of a micro-objective, followed by a pinhole with an aperture of 10 μm. The tested system is situated appropriately behind a collimator, and a microscope is used to take the magnified images. Figure 7 shows the star images captured by the eyepiece from channel –10 to channel 10, while Fig. 8 shows the star images captured on channel 0 as well as at the points with a distance of $\pm$4 mm and $\pm$2 mm off the optical axis respectively. As can be seen, for all the star images, the Airy discs always look good and uniform, which shows the system works well in the full designed FOV and has a loose tolerance on the eccentricity. However, one might note that with the FOV and eccentric distance increasing, the first bright ring of the star image starts to become blurred due to the strong astigmatism caused by the poor alignment between the primary lens and the eyepiece. This can be overcome with careful mounting and alignment of the system.

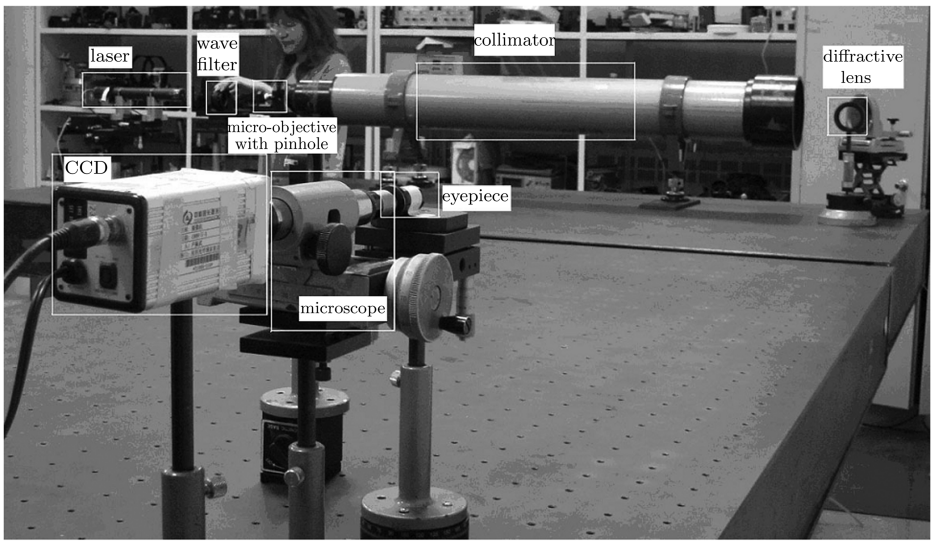


Fig. 6. Star image test system.



Fig. 7. Star images for five typical channels.

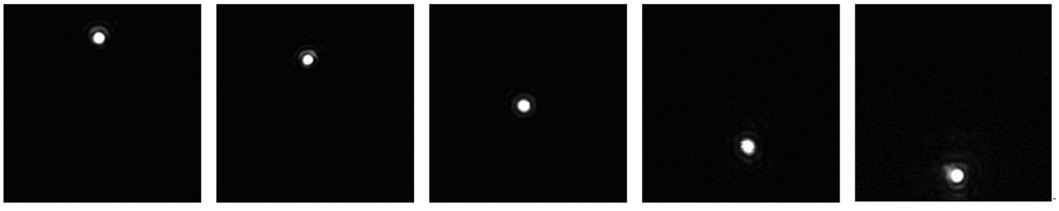


Fig. 8. Star images for the eccentric tolerance of the primary lens.

To test the resolution,[14] the laser, the micro-objective and the pinhole in the optical setup shown in Fig. 6 are replaced by an incandescent lamp, a wave filter and a resolution power test target respectively. By moving the eyepiece from channel 0 to channel 10, resolution images for different channels are obtained with the same part of 200 lp/mm space frequency and are shown in Fig. 9, while Fig. 10 shows the resolution test result of the channel 0 moving from 1 mm to 4 mm off the optical axis. It is obvious that for all of the cases, the images always look clear and there is not much difference in the sharpness of the images between channel 0 and channel 10 or even in the presence of 4 mm eccentricity. Therefore, it can be concluded that the system has a good imaging ability within the designed FOV and has a loose tolerance on the alignment of the components.

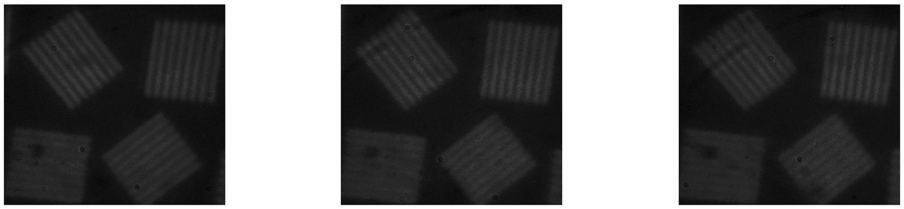


Fig. 9. Resolution images for different channels.

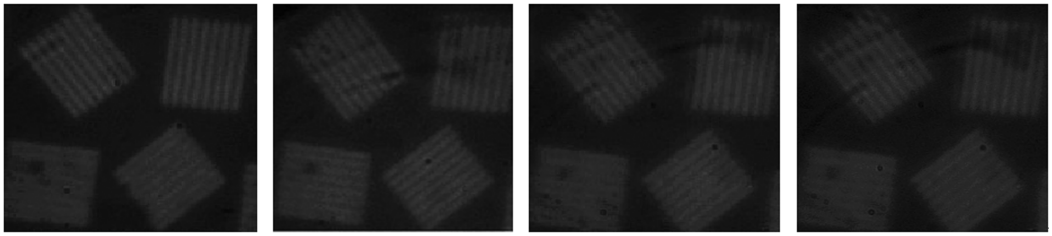


Fig. 10. Resolution images for eccentric tolerance of primary lens.

5. Object imaging of the system

5.1. Structure of the imaging system

The other system with one primary lens and three eyepieces is used to image the distant object. As shown in Fig. 11(a), the primary lens clinging to one part of the window is used to collect light from the target outside the laboratory, and the other part of the window was covered by a black cloth to block stray light. Figure 11(b) shows the arrangement of three eyepieces in detail. With the help of the collimated laser beam, the first eyepiece is axially mounted on the focus of the primary lens, the second eyepiece is situated 2° horizontally away from the first one, and the third eyepiece is located 0.2° horizontally and 0.6° vertically away from the first one to overcome the mechanism limits. Two clear pictures shown in Fig. 12 have been successfully taken by the central and the marginal eyepieces spontaneously, which again proves that the compound diffractive telescope can obtain good-quality images in the full FOV.

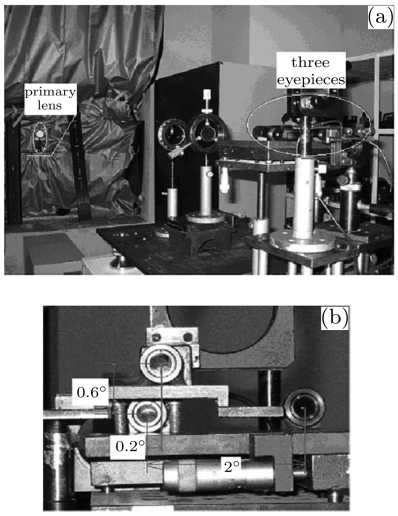
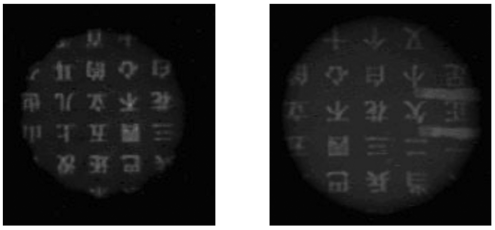


Fig. 11. (a) Object imaging structure of the system, and (b) arrangement of the eyepieces.



(a) (b)

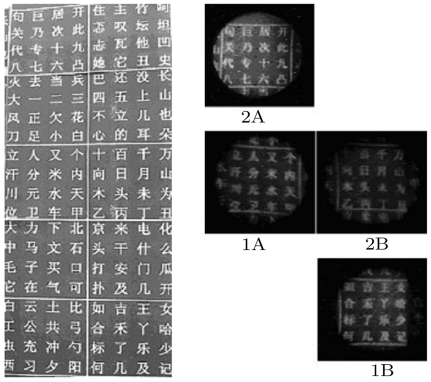
Fig. 12. (a) 0 degree field of view, and (b) 2 degree field of view.

5.2. Image splicing

As the FOV of the compound diffractive telescope is expanded to $\pm 2°$, thus pictures taken from different channels over the whole FOV could be spliced together to comprise a complete image. To demonstrate the splicing of the images, we took the 0° eyepiece and the 0.2° eyepiece as an example here. As in the vertical direction there is 0.6° angle distance between them, there will be a delay in the vertical direction, in that the compound diffractive telescope is a line scanning system along one direction, the delay effect can be eliminated by splicing two images of the target together.

Ten patches of Chinese characters shown in Fig. 13(a) are used as the target. Two pictures, 1A and 1B, are first captured by the two eyepieces. Then both of the eyepieces are moved 0.6° down, and another two pictures, 2A and 2B, are obtained. The obtained four pictures are shown in Fig. 13(b).

It is clear that images 2A and 2B are images of two patches positioned higher than that of images 1A and 1B. Figure 14 shows a combined image spliced together by images 1A and 2B, which proves the availability of image splicing of the system.



(a) (b)

Fig. 13. (a) Chinese character target board outside, (b) four images taken by two eyepieces.

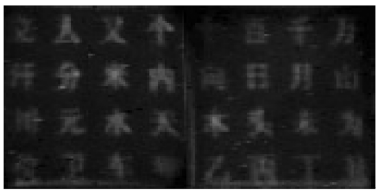


Fig. 14. Image splicing of 1A and 2B.

6. Conclusion

In this paper, a novel space optical system compound diffractive telescope is presented, and it successfully solves the contradiction between light weight and wide FOV. The performance of the system is analysed. A more accurate prediction is provided by the modified phase function model of diffractive optical elements. The system is optimized by stray light analysis. The system can provide nearly diffraction limit imaging within $\pm 2°$ of FOV, so the pictures from adjacent FOV can be spliced together. In future, a larger FOV can be obtained by arranging more sets of the compound diffractive telescope together.

References

[1] Ansbro E 2004 *SPIE* **5489** 1173
[2] Surya C, James D M, Brian G P, Brett D and Dan K M 2005 *SPIE* **5894** 1
[3] Barton L M, Britten J A and Dixit S N 2001 *Appl. Opt.* **40** 447
[4] Hyde R A 1999 *Appl. Opt.* **38** 4198
[5] Horridge G A 1977 *Scientific American* **237** 108
[6] Horridge G A 1980 *Proc. Roy. Soc. London* B **207** 287
[7] Land F 1980 *Nature* **287** 681
[8] Lu Z W, Zhang N, Liu H, Li F Y and Sun Q 2007, *SPIE* **6289** 10
[9] Thibault S, Renaud N and Wang M 1999 *SPIE* **3779** 334
[10] Wang X L, Wu L, Yuan C J and Zhai H C 2007 *Acta Phys. Sin.* **56** 218 (in Chinese)
[11] Zhang H, Liu H, Lu Z W and Zhang H X 2008 *Appl. Opt.* **47** 4055
[12] Wu F T, Jiang X G, Liu B and Qiu Z X 2009 *Acta Phys. Sin.* **58** 3125 (in Chinese)
[13] Liu H, Lu Z W, Yue J Y and Zhang H X 2008 *Optics Express* **16** 16195
[14] Cao Z L, Hu L F, Jiang B G, Li C, Mu Q Q and Xuan L 2008 *Chin. Phys.* B **17** 4529